

# Supplement information

## Potential Barrier in Diffusion of Nanoparticle in Ordered Polymer Network

Yu Lu and Guo-Hui Hu\*

*School of Mechanics and Engineering Science, Shanghai Institute of Applied Mathematics  
and Mechanics, Shanghai Key Laboratory of Mechanics in Energy Engineering, Shanghai  
University, Shanghai, China*

E-mail: ghhu@staff.shu.edu.cn

### S1: Modeling of Polymer network and Nanoparticles

The mesh size  $a_x$  and  $N_{seg}$  follows:

$$a_x \simeq bN_{seg}^\nu, \quad (1)$$

where  $b$  is the length of the Kuhn segment and  $\nu$  is the Flory exponent that depends on the solvent quality. The polymer network is allowed to relax to the thermal equilibrium in athermal solvent before simulation, so that  $\nu = 0.588$ .

Once the number density  $n$  is given, the volume fraction of polymer  $\varphi_p$  can be calculated by three prescribed parameters  $N_{seg}$ ,  $a_x$  and  $n$ . For example, in cubic topology, the volume fraction is  $\varphi_p \approx 3N_{seg}/na_x^3$ . The correlation length  $\xi$  is depended on the volume fraction of polymer  $\varphi_p$  with

$$\xi \simeq b\varphi_p^{-\nu/(3\nu-1)}, \quad (2)$$

so that the tube diameter  $a_e$  can be estimated by  $a_e \approx 5\xi$ .

A parameter  $\theta = a_x/a_e$  is utilized to describe the degree of entanglement. For  $\theta > 1$  ( $a_x > a_e$ ), the polymer network is entangled. For  $\theta < 1$  ( $a_x < a_e$ ), the polymer network is unentangled.

Harmonic bond is used to connect two polymer particles with the bond energy defined by

$$E_{bond} = e_{max} \left( \frac{r}{r_0} - 1 \right)^2, \quad (3)$$

in which  $r_0$  is the equilibrium distance between two monomers and is equal to the Khun length  $b$ , which can be calculated by equation (1).  $e_{max}$  stands for the maximum energy of the bond. This bead-spring model has been widely used in DPD simulations of polymers and gels.<sup>1-4</sup>

In DPD simulations, all the physical quantities are expressed in DPD units, therefore it is necessary to establish the mapping from the real physical scale to the DPD scale. The reference length is based on the mesh size of polymer network,  $L^{ref} = a_x$ . The mass of the solvent particle is considered as the characteristic quantity, and  $k_B T = 1$ .

As recommended by Groot and Warren,<sup>5</sup> the conservative parameters are chosen to be  $a_{ij}^{ss} = a_{ij}^{pp} = \frac{75k_B T}{n} = 25$ , with the superscripts  $s$  and  $p$  representing for solvent and polymer respectively. As polymers are immersed in athermal solvent, thus  $a_{ij}^{sp} = 25$ . The dissipative coefficients are set as  $\gamma_{ij}^c = 4.5$ ,  $\gamma_{ij}^s = 0$  for both s-s, p-p and s-p interactions. Different from the previous study,<sup>6</sup> here we choose shearing dissipative coefficient to be zero because the rotation of the solvent particles has minor effects on the diffusion of NPs. For simplification,  $\lambda_{ij} = 0$  for the interaction between NPs and small (solvent and polymer) particles.

An exponential form weight function equation is used to represent NP-solvent and NP-polymer interaction, in which the factor of weight function  $b_{ij} = -20$ . The NP performs as a solid sphere and the solvent particle cannot penetrate the NP. Radial distribution function (RDF)<sup>7</sup> of solvent and NP,  $g^{sn}(r)$ , which is approximately a step function rapidly increasing from 0 to 1, as shown in Fig. S1, is calculated to measure the effective radius of solid sphere,

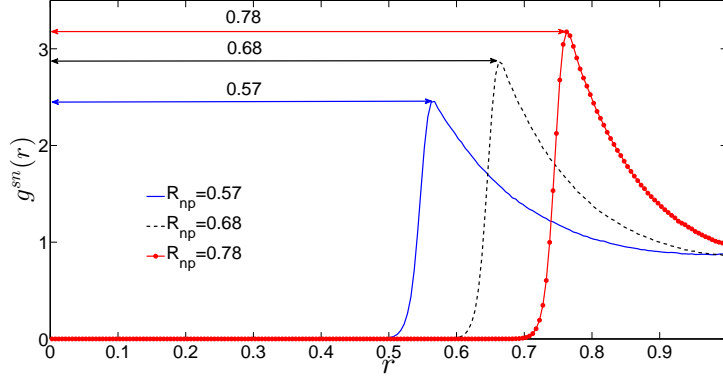


Figure S1: Radial distribution function  $g^{sn}(r)$  when radius of solid part are 0.5, 0.6 and 0.7. The effective radius is the peak location of  $g^{sn}(r)$ , 0.57, 0.68 and 0.78.

and the effective radius is the location of the peak of  $g^{sn}(r)$ .

Conservative force parameter  $a_{ij}$  is adjusted to obtain desired solid radius. Specifically, as shown in Fig. S2(a), The effective radius  $R_{np}$  is dependent linearly on the conservative parameter  $a_{ij}$ , and the linear fitting curve is given by

$$a_{ij} = 56.81 + 130.3R_{np}. \quad (4)$$

The dissipative coefficients for both NP-solvent and NP-polymer interaction are chosen as  $\gamma_{ij}^c=3.5, \gamma_{ij}^s=5.5$  following Pan et al.<sup>8</sup> To obtain proper hydrodynamic Stokes resistance exerted on NP,  $r_{cut,D}$  is used to yield diffusion coefficient of NP in pure solvent satisfying Einstein-Stokes relation given by  $D_0 = kT/6\pi\eta_s R_{np}$ , in which  $\eta_s = 1.8368$  is viscosity of pure solvent, which is calculated from reverse Poiseuille flow following approach in Ref.<sup>9</sup> To reach the target diffusivity, cut-off radius of dissipative force  $r_{cut,D}$  should satisfy a linear relation varying with  $R_{np}$ ,

$$r_{cut,D} = 0.4311 + 0.7134R_{np}, \quad (5)$$

which is plotted in the Fig. S2(b).

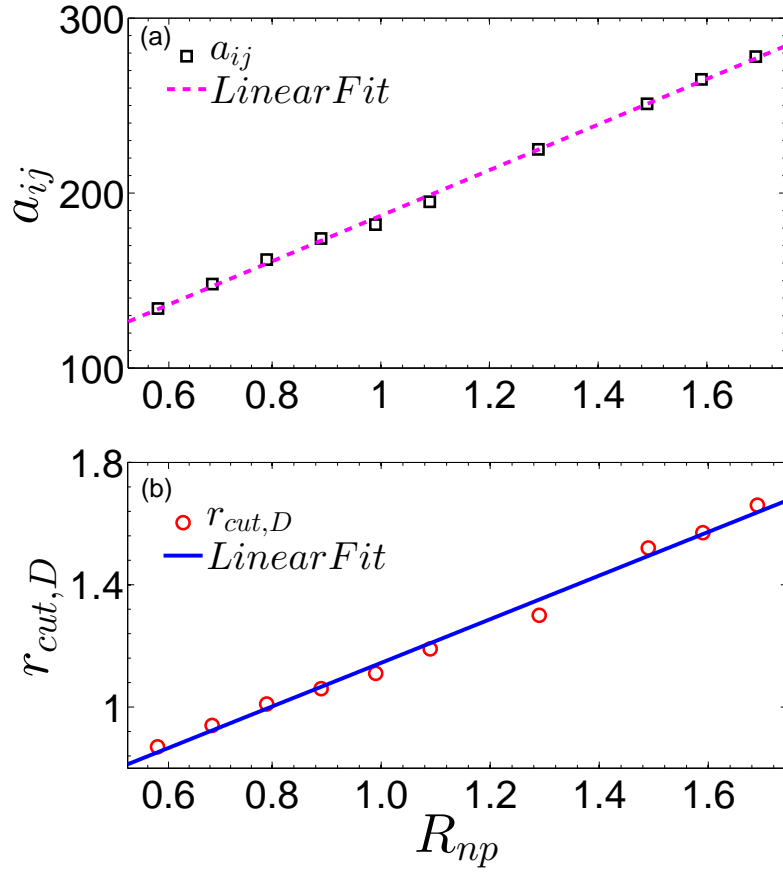


Figure S2: (a) Conservative parameter  $a_{ij}$  and (b) cut-off radius of dissipative force  $r_{cut,D}$  versus radius of NP  $R_{np}$ . Conservative parameter  $a_{ij}$  is adjusted to obtain desired effective NP radius. Cut-off radius of dissipative force  $r_{cut,D}$  is chosen to correct the hydrodynamic force.

## S2: Trajectory of NP diffusion

Typical 3D trajectory of NP hopping are shown in Figure S3, which shows the long displacement in a short time. The hopping length is equal to the mesh size  $a_x$ . This phenomenon can be indicated by the multi-peaks in DPDF.

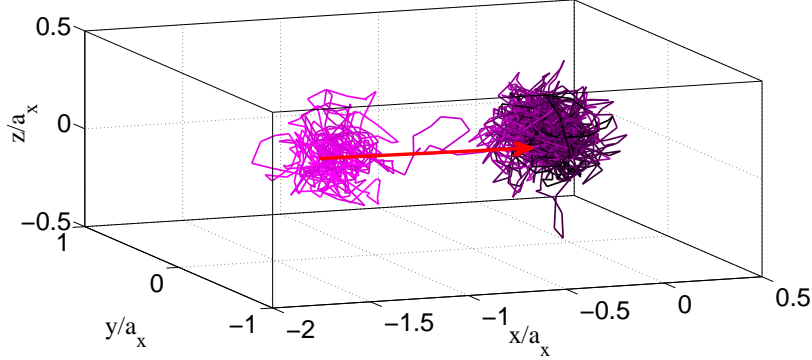


Figure S3: Typical 3D trajectories for NP hopping.

## S3: Potential Barrier during hopping process

In order to calculate potential barrier during hopping process, a large number of ensemble averaging and fitting are conducted in the present study. The interval  $(0.0 < X_l < 0.5)$  is divided into several bins with width of  $\delta r$ . Then  $\rho(X_l)F(X_l)$  and  $\rho(X_l)$  for each bins "i" can be obtained directly,

$$\rho(X_{li})F_{hop}(X_{li}) = \frac{1}{N_{hop}} \sum_{j=1}^{N_i} F_j(X_{lij} | X_{li} < X_{lij}/a_x < X_{li} + \delta r), t_j \in T_{hop},$$

$$\rho(X_{li}) = \frac{N_i}{N_{hop}}$$

where  $j$  denote the timestep in bin  $i$ .

As shown in Figure S4(a)(b),  $\rho(X_l)$  and  $\rho(X_l)F_{hop}(X_l)$  is plotted against  $X_l/a_x$ . It should mention that, when  $X_l$  is close to one, the samples in those pieces might be very small, which results in a large fluctuation in  $\rho(X_l)F_{hop}(X_l)$ . To overcome this difficulty,

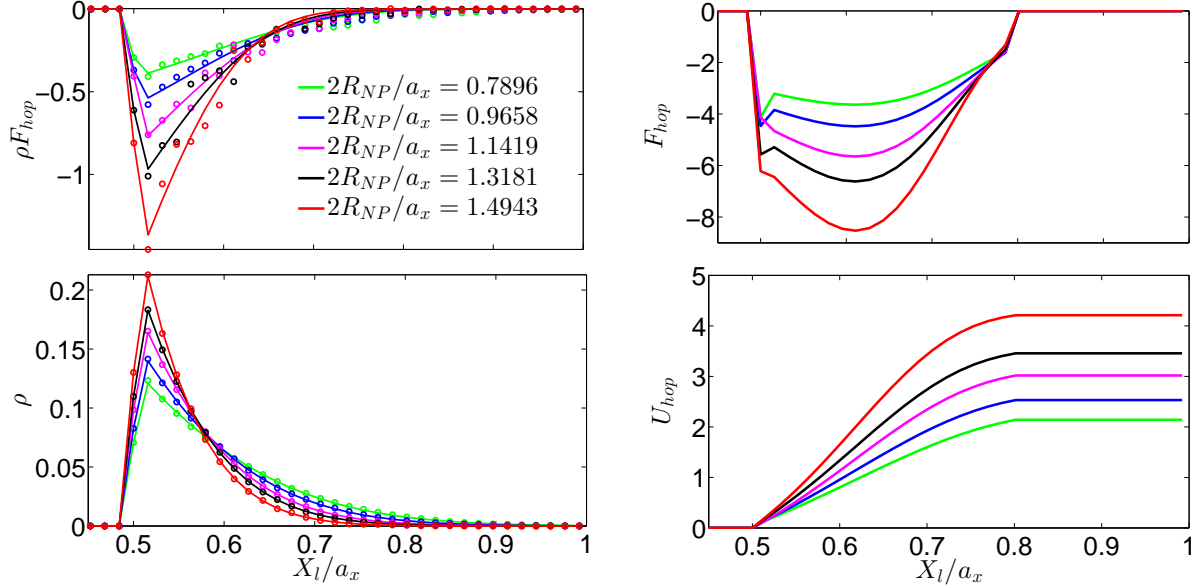


Figure S4: (a)  $\rho(X_l)$  and (b)  $\rho(X_l)F_{hop}(X_l)$  is plotted against the  $X_l/a_x$ . (c)  $F_{hop}(X_l)$  is calculated by the fitting function of  $\rho(X_l)F_{hop}(X_l)$  divided by  $\rho(X_l)$ . (d)  $U_{hop}(X_l)$  is the associated potential energy.

$\rho(X_l)$  and  $F_{hop}(X_l)$  are fitted by proper functions. The  $\rho(X_l)$  can be satisfactorily fitted with an exponential function  $Aexp(-k_1X_l^\alpha)$  ( $A$ ,  $k_1$ , and  $\alpha$  are coefficients). Considering the function form used for fitting and the weight of the loss function might have a certain impact on the final result, the fitting of  $\rho(X_l)F_{hop}(X_l)$  needs to follow the following principles: (a) as  $F_{hop}(X_l)$  must be bounded, the decay speed of  $\rho(X_l)F_{hop}(r)$  ( $Bexp(-k_2X_l^\beta)$ ,  $B$ ,  $k_2$ , and  $\beta$  are coefficients) should be greater than  $\rho(X_l)$ , that is  $\beta > \alpha$ ; (b) since  $\rho(X_l)F_{hop}(X_l)$  might fluctuate profoundly when  $X_l$  is close to 1, the weight function of the loss function needs to be a decreasing function to eliminate the influence of fluctuations on the fitting.

## References

- (1) Yong, X.; Kuksenok, O.; Matyjaszewski, K.; Balazs, A. C. Harnessing interfacially-active nanorods to regenerate severed polymer gels. *Nano Letters* **2013**, *13*, 6269–6274.
- (2) Gnan, N.; Rovigatti, L.; Bergman, M.; Zaccarelli, E. In silico synthesis of microgel particles. *Macromolecules* **2017**, *50*, 8777–8786.

- (3) Schlijper, A.; Hoogerbrugge, P.; Manke, C. Computer simulation of dilute polymer solutions with the dissipative particle dynamics method. *Journal of Rheology* **1995**, *39*, 567–579.
- (4) Nikolov, S.; Fernandez-Nieves, A.; Alexeev, A. Mesoscale modeling of microgel mechanics and kinetics through the swelling transition. *Applied Mathematics and Mechanics* **2018**, *39*, 47–62.
- (5) Groot, R. D.; Warren, P. B. Dissipative particle dynamics: Bridging the gap between atomistic and mesoscopic simulation. *The Journal of Chemical Physics* **1997**, *107*, 4423–4435.
- (6) Wang, Y.; Ouyang, J.; Li, Y. Parametric study of fluid–solid interaction for single-particle dissipative particle dynamics model. *Microfluidics and Nanofluidics* **2018**, *22*, 78.
- (7) Schmidt, J.; Skinner, J. Brownian Motion of a Rough Sphere and the Stokes- Einstein Law. *The Journal of Physical Chemistry B* **2004**, *108*, 6767–6771.
- (8) Pan, W.; Pivkin, I. V.; Karniadakis, G. E. Single-particle hydrodynamics in DPD: A new formulation. *Epl (Europhysics Letters)* **2008**, *84*, 548–551.
- (9) Backer, J.; Lowe, C.; Hoefsloot, H.; Iedema, P. Poiseuille flow to measure the viscosity of particle model fluids. *The Journal of Chemical Physics* **2005**, *122*, 154503.